Turner, GF.; Campbell, F.; Moggach, SA.; Parsons, S.; Goeta, AE.; Muñoz Roca, MDC.; Real, JA. (2020). Single-Crystal X-Ray Diffraction Study of Pressure and Temperature-Induced Spin Trapping in a Bistable Iron(II) Hofmann Framework. Angewandte Chemie International Edition. 59(8):3106-3111. https://doi.org/10.1002/anie.201914360

Single-Crystal X-Ray Diffraction Study of Pressure and Temperature-Induced Spin Trapping in a Bistable Iron(II) Hofmann Framework

Gemma F. Turner, Fallyn Campbell, Stephen A. Moggach, Simon Parsons,* Andr8s E. Goeta†,* M. Carmen Muñoz, and Josᶒ A. Real**

Abstract: High-pressure single-crystal X-ray diffraction has been used to trap both the low-spin (LS) and high-spin (HS) states of the iron(II) Hofmann spin crossover framework, [Fe^{II}(pdm)(H$_2$O)[Ag(CN)$_2$]$_2$·H$_2$O, under identical experimental conditions, allowing the structural changes arising from the spin-transition to be deconvoluted from previously reported thermal effects.

Iron(II) spin crossover (SCO) complexes reversibly switch between the low-spin (LS, $t_{2g}^6e_g^0$) and high-spin (HS, $t_2{}^4e_g^2$) electronic states in response to a change in temperature, pressure and irradiation with light.[1–8] The HS–LS switch involves population–depopulation of the antibonding e_g orbitals, thereby inducing a lengthening or shortening of the Fe^{II}@L bonds by ca. 0.2 c. These structural changes are transmitted from one active SCO building block to another across the crystal through elastic interactions. Strong coupling between the active building blocks favours cooperative hysteretic behaviour, conferring bistability (memory effect) to the magnetic, optical, electrical, structural and mechanical properties of the material. These properties are promising for the application of SCO materials in data storage devices, sensors and actuators.[9–11]

Thermally induced SCO is an entropy driven process. The energy gap between the low-lying LS state and the HS state is thermally compensated due to the larger entropy (mainly vibrational) associated with the longer Fe@L bonds characteristic of the HS state, which is stabilised at high temperatures by the term, $T\Delta S_{HL}$. In contrast, since the characteristic volume of the HS state, V_{HS}, is invariably larger than that of the LS state, V_{LS} ($\Delta V_{HL} = V_{HS}@V_{LS} > 0$), pressure ($p$) destabilises the HS state, increasing the energy gap by ca. $p\Delta V_{HL}$ with respect to the LS state. The equilibrium temperature, $T_{1/2}(p)$ ($\Delta G_{HL} = 0$), at which the molar fractions g_{HS} and g_{LS} are equal to $^1/_2$, increases following the Clausius–Clapyron equation: $T_{1/2}(p) = T_{1/2} + p\,[\Delta V_{HL}/\Delta S_{HL}]$, where $T_{1/2}$ is the equilibrium temperature at ambient pressure. Besides this linear increase of $T_{1/2}(p)$, pressure imparts significant changes to the cooperative properties, such as modification of the hysteresis width, introduction of steps in the hysteresis loop, stabilisation of the HS state, or even induction of SCO in inert metal centres.[12]

Unlike thermally-driven SCO studies, work on the effect of pressure on SCO complexes is relatively rare due to experimental constraints.[12] This is particularly true for single crystal X-ray diffraction studies because, in addition to intrinsic technical difficulties, molecular SCO materials are sensitive to low pressures (< 0.1 GPa), which are difficult to control. Only six single crystal structure determinations of SCO complexes under pressure have been reported so far.[14–19]

Incorporation of Fe^{II} SCO building blocks into coordination polymers has proven to be an effective synthetic approach to find new, bistable SCO materials.[3,20] In particular, Hofmann frameworks containing SCO Fe^{II} linked by di- or tetracyano-metallate complexes have contributed to the development of the field of SCO, with relevant examples of stimulation of the SCO centres by light, temperature, pressure, or even with analytes, affording, in some cases, switchable behaviour with a wide region of bistability.[21,22] Among them, the three-dimensional (3D) Hofmann SCO coordination polymer [Fe^{II}(pmd)(H$_2$O)][Ag(CN)$_2$]$_2$·H$_2$O (pmd = pyrimidine) (FeAg) displays exceptional SCO properties.[23] Previous work has shown that the magnetic and optical properties of FeAg show pressure-tuneable thermal hysteretic behaviour in a wide temperature window (ca. 210 K < T > 350 K) without losing its well-defined square shape

[*] G. F. Turner, Dr. S. A. Moggach
School of Molecular Sciences/Centre for Microscopy, Characterisation and Analysis, The University of Western Australia
35 Stirling Highway, Crawley, Perth, WA, 6009 (Australia)
E-mail: stephen.moggach@uwa.edu.au

Dr. F. Campbell, Prof. S. Parsons
EastChem School of Chemistry and Centre for Science at Extreme Conditions, The University of Edinburgh
Kings Buildings, West Mains Road, Edinburgh, EH9 3JJ (UK)
E-mail: s.parson@ed.ac.uk

Dr. A. E. Goeta
Department of Chemistry, Durham University
South Road, Durham, DH1 3LE (UK)

Prof. M. C. MuÇoz
Departamento de Fłsica Aplicada, Universitat PolitHcnica de ValHncia
Camino de Vera s/n, 46022 Val8ncia (Spain)

Prof. J. A. Real
Institut de Ciencia Molecular/ Departament de Quimica Inorganica, Universitat de ValHncia
Doctor Moliner 50, 46100 Burjassot, ValHncia (Spain)
E-mail: jose.a.real@uv.es

[†] Deceased

(Figure S3a in the Supporting Information).[24] Interestingly, the $T_{1/2}(p)$ values extracted from the heating and cooling modes of the thermal hysteresis curves are differently affected by pressure, displaying a non-linear region characterised by a hysteretic dependence on pressure (Figure S3b).[24] Here, we report for the first time both the LS and HS high pressure structures (0.5 GPa) of FeAg under identical experimental conditions by taking advantage of the bistable nature of its SCO properties using a combination of temperature and pressure. This allowed us to identify the structural changes caused solely by the spin-transition (albeit at high-pressure), which previously has only generally been possible at very low temperatures using light-induced excited spin-state trapping studies (LIESST).[25]

Let us briefly recall the crystal structure of the HS and LS states of FeAg obtained at 225 K and 120 K at ambient pressure, respectively.[23] The $P2_1/c$ crystallographic symmetry is retained in both the HS and LS states although considerable changes to the local complex structure upon undergoing the spin-transition are reported. FeAg forms a triply-interpenetrated 4-connected open framework with a wine-rack cds ($CdSO_4$) topology (Figure 2 a,b). Two symmetrically independent Fe^{II} centres (Fe1 and Fe2) with axially coordinated pyrimidine (pmd) or water ligands, respectively, are connected by μ_2-$[Ag(CN)_2]^{-}$ linkers in infinite polymeric chains, forming a layer of edge-sharing {-Fe1-CN-Ag1-CN-Fe2-CN-Ag2-CN-} rectangular motifs. Pillaring cyano-silver anions extend the framework in three-dimensions.

The space between the interpenetrated nets is occupied by four equivalent extra-framework water molecules per unit cell. Each water molecule is positioned between two ligated waters at Fe2 centres in adjacent nets, forming a network of hydrogen bonds between interpenetrated frameworks along the *c*-axis. Parallel to the network of hydrogen bonds, π–π interactions between neighbouring pmd ligands on adjacent Fe1 centres propagate the crystal (Figure S4). The nets are further connected by infinite zig-zag chains of silver atoms that propagate the *c*-axis. Argentophilic[26] interactions between intra-chain Ag atoms (Ag1···Ag1 < 3.6 Å) extend along the direction of the one-dimensional chain (Figure S4).

Hydrostatic pressure was applied to a single crystal of FeAg in its yellow HS state in a miniature Merrill–Bassett diamond anvil cell[27] in a mixture of methanol/ethanol as the pressure-transmitting medium (PTM). The pressure was determined by the ruby fluorescence method.[28] The crystal is in the HS form under ambient conditions but it could be converted to the LS form by increasing the pressure to 0.7 GPa, resulting in a piezochromic colour change from yellow to red (Figure 1 c). X-ray diffraction data were then collected after lowering the applied pressure to 0.5 GPa and increasing the temperature to 323 K using an Oxford Cryosystems Cryostream Plus low-temperature device (chapter 1.2 in the Supporting Information), where the LS state was retained. This was confirmed by retention of the red colour of the crystal. A spin-transition from LS to HS occurred upon heating the sample to 368 K at 0.5 GPa. Diffraction data were then collected after cooling the sample to 323 K, where the HS state was retained, confirmed by retention of the yellow colour of the crystal. We found that the diffraction data had to be collected at 323 K, otherwise the HS–LS transition occurred spontaneously.

This demonstrates that the SCO properties of FeAg at 0.5 GPa correspond to a hysteretic behaviour that retains both spin states at identical thermodynamic coordinates (T, p) (bistability), and agrees reasonably well with the data linearly extrapolated from the upper part of the previously reported hysteresis curve of the $T_{1/2}$ vs. p plot,[24] represented by broken lines in Figure 1 b. This extrapolation indicates that at 0.5 GPa FeAg should display a cooperative SCO with $T_{1/2}^{down} \approx 327$ K and $T_{1/2}^{up} \approx 340$ K (hysteresis $\Delta T \approx 13$ K). This value of $T_{1/2}^{down}$ is slightly larger than the 323 K at which FeAg retains the HS and LS states but is close to the real $T_{1/2}^{down}$. The same estimation for the experimental SCO $\chi_M T$ vs. T plot at 0.34 GPa (Figure S3b) gives calculated values of $T_{1/2}^{down} \approx 303$ K and $T_{1/2}^{up} \approx 325$ K ($\Delta T \approx 22$ K), which compare well with the experimental values of $T_{1/2}^{down} = 302$ K and $T_{1/2}^{up} = 326$ K ($\Delta T \approx 24$ K).

Crystallographic and structural data for FeAg at 323 K and 0.5 GPa in the LS and HS states are given in Table 1. The measured bond lengths in the HS phase are less precise than in the LS phase since the crystal has undergone two phase transitions, which caused slight damage to the crystal.The absence of disorder in the measured crystal structures indicates full conversion between the spin-states during the spin-crossover.

During the LS to HS transition, the Fe1 octahedral coordination volume (ΔV_{Fe1} in Table 1) increased by 3.07 Å^3 (30 %). As expected, the Fe2 centre is SCO-inactive at 0.5 GPa ($\Delta V_{Fe2} = 0.46$ Å^3, 3.5 %) due to the weak ligand field strength associated with the axially coordinated water molecules. This is confirmed by retention (or lack of expansion) of the Fe2@N or Fe2@O bond distances (Table S5).

The coordination environment of Fe1 contains three symmetrically independent bonds: two equatorial N-donor cyano-ligands, Fe1@N1 and Fe1@N2, and an axial bond to an N-coordinated pyrimidine ligand, Fe1@N3. The LS to HS transition caused each of the Fe1@N coordination bonds to lengthen by different amounts (Table 1). Statistically significant lengthening of the respective equatorial Fe1@N1 and Fe1@N2 (cyano ligand bonds) from 1.947(11) Å to 2.11(3) Å (8.4 %) and from 1.950(10) Å to 2.12(2) Å (8.7 %) occurs, and is responsible for the expansion of the $[Fe1Fe2\{Ag(CN)_2\}]_n$ polymeric chains and extension of the *a* and *b* unit cell axes. Lengthening of the axial coordination bond to pyrimidine, Fe1@N3, from 2.026(9) Å to 2.25(2) Å (11.1 %) is also observed.

These changes to the $[Fe1N_6]$ bond lengths result in a pronounced distortion of the Fe1 octahedral coordination geometry in the HS state, with the distortion angle in the LS state, $\Sigma_{LS} = 9.2(8)°$ (defined as the sum of the deviation of the N-Fe1-N *cis* coordination angles away from 90°) increasing to $\Sigma_{HS} = 22.6(2)°$ (146 %) after the spin-transition. The result in an elongated coordination octahedron of Fe1 in the HS state as the equatorial diameter of the octahedron (N1-Fe1-N1) increased by 0.34(3) Å (8.7 %) whilst the axial diameter (N3-Fe1-N3) increased by 0.45(3) Å (11.1 %) during the LS to HS transition (Table S11).

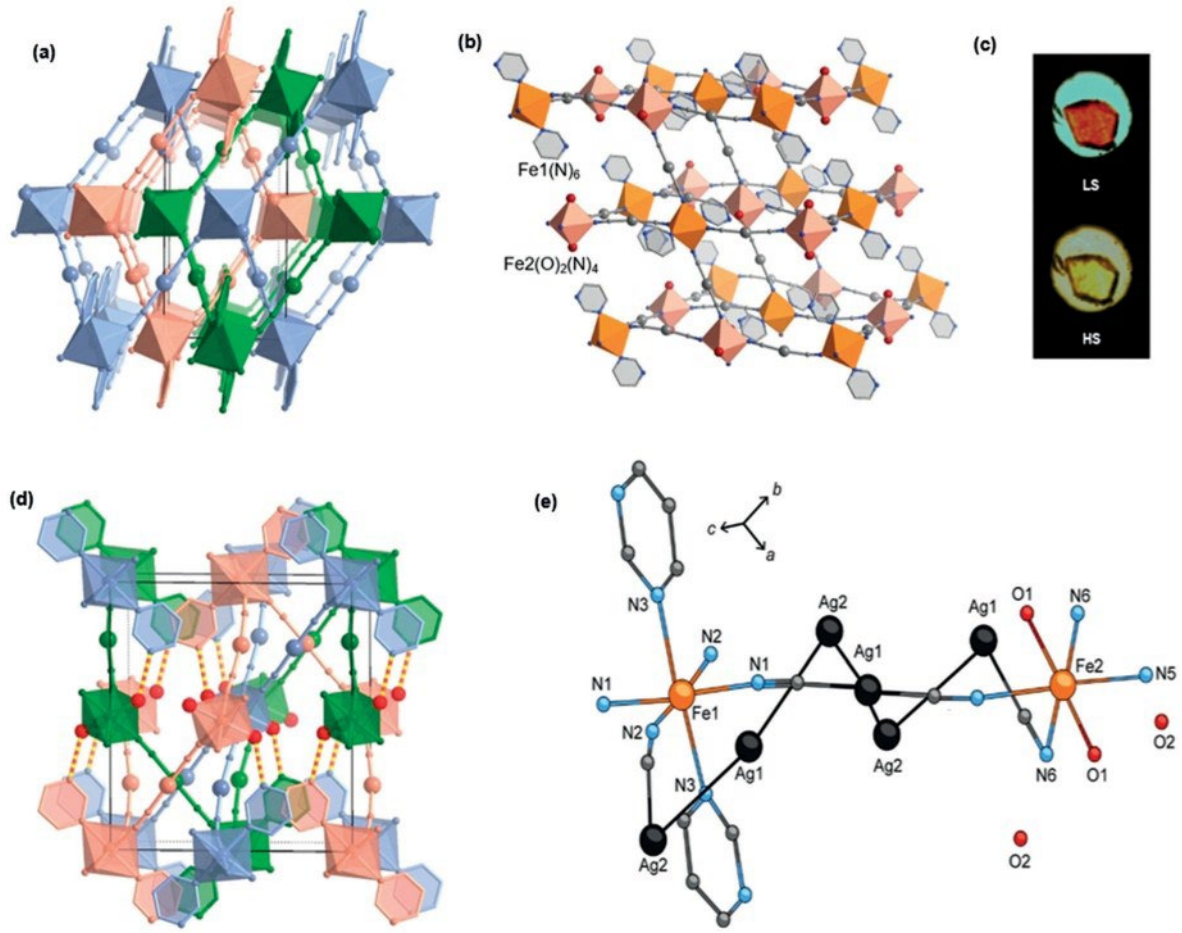

Figure 1. a) Fragment of the triply interpenetrated frameworks of FeAg. Individual nets are coloured, blue, salmon, green. b) Fragment of one net showing the cds topology. The two type of octahedrons [FeN_6] and [FeN_4O_2] have been marked with orange, and light-red colours. The oxygen atom of the coordinated water molecule is coloured in red. c) Colour of the crystals in the LS and HS states. d) Perspective view of a fragment of the triply interpenetrated frameworks interconnected through the hydrogen bonds between the uncoordinated N-atom of pyrimidine and the coordinated water molecule (red-yellow bars). Uncoordinated water molecules are not shown. e) Fragment of FeAg showing molecular connectivity. H-atoms are removed for clarity.

Table 1: Crystallographic and structural data for FeAg in the LS and HS under identical conditions of temperature and pressure, and for the thermally induced spin-transition reported by Niel et al. (Ref. [23]).

	LS[a]	HS[a]	D [%][a]	LS (120 K)[b]	HS (225 K)[b]	D [%][b]
a [b]	14.308(8)	14.739(14)	+ 3.01	14.2584(4)	14.7035(5)	+ 3.12
b [b]	13.004(4)	13.203(5)	+ 1.53	13.0528(3)	13.2962(5)	+ 1.86
c [b]	7.3758(19)	7.218(3)	@2.14	7.493(2)	7.3852(3)	@1.44
b [**8**]	91.81(3)	90.99(6)	@0.89	92.055(10)	91.441(2)	@0.67
V [b³]	1371.67(1)	1404.4(16)	+ 2.39	1393.64(4)	1443.35(5)	+ 3.57
Fe1-N1 [b]	1.947(11)	2.11(3)	+ 8.37	1.931(2)	2.1384(19)	+ 10.72
Fe1-N2 [b]	1.950(10)	2.12(2)	+ 8.72	1.930(2)	2.132(2)	+ 10.47
Fe1-N3 [b]	2.026(9)	2.25(2)	+ 11.06	1.993(2)	2.2237(17)	+ 11.59
V_{Fe1} [b³][c]	10.241	13.310	+ 29.97	9.897	13.492	+ 36.32
$S_{LS/HS}$ [**8**]	13.8	35.6	+ 157.97	12.92	20.48	+ 58.51
f [**8**][e]	@136.0(7)	143.4(11)	+ 5.. 4	135.1(2)	140.7(2)	+ 4.15

[a] This work (*T* = 323 K, *P* = 0.5 GPa). [b] Ref. [15] (*T* = 120 K (LS), 225 K (HS), *P* = ambient). [c] Octahedral coordination volume (PLATON).

Comparable structural changes in the pyrimidine-ligated Fe1 centre were reported by Niel et al. for the temperature-induced LS to HS transition at 120 K and 225 K (Table 1).[23] The thermally-induced spin-transition caused the [Fe1@N_6] bonds to extend by an additional 2.4 %, 1.8 % and 0.5 % for Fe1@N1, Fe1@N2 and Fe1@N3 bonds, respectively, due to increased thermal motion. Extension of the Fe1@N bonds was accompanied by a volumetric expansion of the octahedral

coordination environment of Fe1, which increased by an additional 6.4 % compared with the deconvoluted spin-transition here reported.

Whilst the thermal-SCO exaggerated the increase in bond distances and coordination volume of Fe1, the octahedral geometry became less distorted in the HS state (Σ_{LS} = 12.92°, Σ_{HS} = 20.48°) than was observed the spin-transition reported here. Evidently, pressurising the material at 0.5 GPa during the LS to HS transition attenuates the SCO-induced [Fe1@N_6] bond lengthening and increases the geometrical deformation about the SCO metal centre. The overall change of the average [Fe1@N_6] bond lengths upon SCO, 0.186(4) Å, agrees well with what is expected for a complete SCO behaviour in an iron(II) complex. However, this value is 13 % smaller than observed for the thermally investigated SCO conversion (0.214(4) Å).[23]

The expansion of the [Fe1@N_6] octahedron upon LS to HS spin-transition at 0.5 GPa is accompanied by an increase in the unit cell volume by 32.7 Å^3 (2.4 %) and a lengthening of the *a* and *b* axes by 3.0 % and 1.5 %, respectively. Extension of the *a* and *b* axes is coincident with the polymeric chains [Fe_2{$Ag(CN)_2$}]$_n$) containing the SCO Fe^{II} centres, which propagate the body diagonal of the unit cell. As is expected for wine-rack topologies,[29] extension of the *a* and *b* axes causes a contraction of the *c* axis by 2.1 %. Topologically, this results in a decrease in the hinge angle of the framework, θ, (defined as N1-Fe1-N2) by 3.3(10)° (3.8 %) (Table S5), resulting in a more compressed wine-rack topology in the HS state (Figure 2). It is worth noting that the distortion of the wine-rack topology due to anisotropic extension of the intersecting Fe1Fe2{$Ag(CN)_2$}]$_n$ chains is not observed in the thermal-SCO of FeAg and hence is exclusively induced by pressure.

The *c* axis is aligned with the strong hydrogen bonds stabilised between the uncoordinated pmd-N atom and the two water molecules *trans* coordinated to Fe2, argentophilic interactions and π–π interactions of pmd ligands of adjacent frameworks (see Figure 2d and Figure S3), making it compliant to contraction. Indeed, the shortening of the *c*-axis coincides with compressible argentophilic Ag1···Ag1 contacts in the silver chains (Table S5). A shortening of the Ag1···Ag1 distance by 0.081(6) Å (2.2 %) and a tightening of the "zig zag" ∠ Ag1-Ag2-Ag1 of the chain (referred to as φ) by 1.57(8)° (2.2 %) brings the centroids of pmd ligands on adjacent interpenetrated frameworks closer together, increasing their π–π interaction (Table S5). The approaching pyrimidine rings rotate about their Fe1-coordination axis (defined by the N1-Fe1-N3-C6 torsional angle), by 7.4(7)° (5.4 %) to adopt a face-to-face configuration of the interacting π-systems. Compression of the H-bond network between the free and ligated water atoms is also observed, with the O1···O2 distances decreasing by up to 1.2 % (Table S7).

Despite a similar volumetric expansion of the Fe1 octahedral coordination volume between the spin-transition reported here and the thermal study by Niel et al. (ca. ΔV_{Fe1} = 30.0 % vs. 36.3 % at 323 K/0.5 GPa, and 120 K/225 K, respectively) a less pronounced shortening of the *c* axis is observed in thermal LS (120 K) and HS (225 K) crystal structures when compared to those under identical experimental conditions.

This attenuated contraction of the *c* axis arises from the "expansion" of the non-covalent interactions probably due to the addition of thermal motion in the silver chains and H-bonding network.[23] A reduction in the intra-chain Ag1···Ag1 distance of 0.05 Å (1.4 %) and a tightening of the Ag1-Ag2-Ag1 zig-zag angle, φ, by 1.2° (1.7 %) was reported, which is 0.5–0.8 % less for both parameters than for the spin-transition here reported.

As a result, the pyrimidine ligands were not brought as close together and did not rotate by as much to increase their π–π interaction, closening (pmd···pmd) and twisting (φ) by 0.55 % and 3.74 % less than for the spin-transition here reported (Table 1). Consequently, uncoordinated water molecules in the crystal were affected by temperature, becoming further apart in the heated HS state in contrast to the

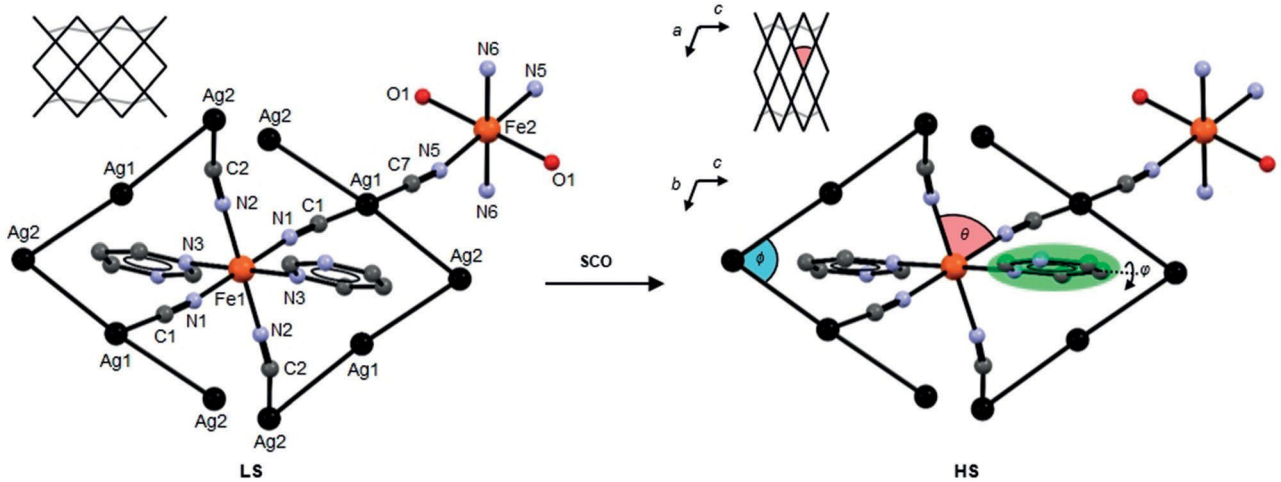

Figure 2. Fragment of FeAg viewed along the *a*-axis in the LS (left) and HS state (right) with zig-zag Ag1-Ag2-Ag1 angle, φ (blue), pyrimidine ligand twist angle, φ, and the N2-Fe1-N1 wine-rack hinge angle, θ (red) labelled. H-atoms are removed for clarity. Top left inset shows the wine-rack topology viewed along the *b*-axis in each spin-state, with the silver chains (grey) and hinge angle (red) highlighted. Contraction of the framework is exaggerated for clarity.

compression reported here (Table S7). The distance between the free and ligated water molecules (O1···O2) increased by up to 1.3 % in the thermal SCO, compared with a decrease of up to 1.2 % for the spin-transition reported here, indicating the thermal dependence of the H-bonding network in FeAg, which may affect the enthalpic and entropic properties of the SCO.

In summary, we have demonstrated that the LS and HS states of FeAg can be trapped under identical experimental conditions of temperature and pressure, allowing the structural changes in the framework caused solely by the spin crossover at 323 K and 0.5 GPa to be characterised. The LS to HS transition results in an expansion of the unit cell and an anisotropic distortion of the lattice parameters.

Extension along the *a* and *b* axes and the increase in the unit cell volume is caused by the expansion of one of the symmetrically independent Fe^{II} centres (Fe1) and is facilitated by the wine-rack topology of the framework. Reduction of the *c*-axis is facilitated by the network of compressible non-convalent interactions parallel to it. Unequal extension of the intersecting $[Fe_2\{Ag(CN)_2\}]_n$ chains of the framework form a distorted wine-rack topology in the HS state. When the LS to HS spin-transition is stimulated by heating FeAg from 120 K to 225 K, as reported by Niel et al., the expansion of the unit cell parameters are exaggerated and the contraction of the *c*-axis is lessened due to the convolution of the spin-transition with thermal effects. Extension along the intersecting $[Fe_2\{Ag(CN)_2\}]_n$ chains is uniform, preventing distortion of the wine-rack topology (Table S*6*).

This study presents only the second SCO system in which the structural changes caused by the spin transition have been deconvoluted[30] from the external stimulus, and is the first to trap both spin states under identical experimental conditions using a combination of temperature and pressure.

These observations demonstrate the importance of deconvoluting the spin-transition from the external stimulus when describing the effect of spin crossover on the structure of materials. This has allowed us to show structural changes imparted by the spin-transition alone, leading to an improved understanding of spin crossover phenomena.

Acknowledgements

This work was supported by the Spanish Ministerio de Economia *y* Competitividad (MINECO), FEDER (CTQ2016-78341-P), Unidad de Excelencia Mar‰a de Maeztu (MDM 2015-0538), the Generalitat Valenciana through PROMETEO/2016/147, and the EPSRC through EP/D503744 and GR/M81830. The authors acknowledge the facilities, and the scientific and technical assistance of the Australian Microscopy & Microanalysis Research Facility at the Centre for Microscopy, Characterisation & Analysis, The University of Western Australia, a facility funded by the University, State and Commonwealth Governments. G.F.T. acknowledges the Australian Government for the provision of an Australian Government Research Training Program (RTP) scholarship.

Conflict of interest

The authors declare no conflict of interest.

Keywords: iron complexes · high-pressure crystallography · Hofmann framework · spin-crossover

[1] E. Kçnig, *Struct. Bonding (Berlin)* 1991, *76*, 51– 152.
[2] P. Ggtlich, A. Hauser, H. Spiering, *Angew. Chem. Int. Ed. Engl.* 1994, *33*, 2024 – 2054; *Angew. Chem.* 1994, *106*, 2109 – 2141.
[3] J. A. Real, A. B. Gaspar, V. Niel, M. C. MuÇoz, *Coord. Chem. Rev.* 2003, *236*, 121 – 141.
[4] *Topics in Current Chemistry*, *Vol. 233* (Eds.: P. Ggtlich, G. Goodwin), Springer, Heidelberg, 2004, pp. 234 – 235.
[5] J. A. Real, A. B. Gaspar, M. C. MuÇoz, *Dalton Trans.* 2005, 2062 – 2079.
[6] M. A. Halcrow, *Polyhedron* 2007, *26*, 3523 – 3576.
[7] A. Bousseksou, G. Moln#r, L. Salmon, W. Nicolazzi, *Chem. Soc. Rev.* 2011, *40*, 3313 – 3335.
[8] C.-M. Jureschi, J. Linares, A. Boulmaali, P. R. Dahoo, A. Rotaru, Y. Garcia, *Sensors* 2016, *16*, 187 – 196.
[9] M. Cavallini, I. Bergenti, S. Milita, J. C. Kengne, D. Gentili, G. Ruani, I. Salitros, V. Meded, M. Ruben, *Langmuir* 2011, *27*, 4076 – 4081.
[10] P. N. Martinho, C. Rajnak, M. Ruben in *Spin-Crossover Materials: Properties and Applications* (Ed.: M. A. Halcrow), Wiley, Oxford, 2013, pp. 376 – 404.
[11] G. Moln#r, S. Rat, L. Salmon, W. Nicolazzi, A. Bousseksou, *Adv. Mater.* 2018, *30*, 1703862.
[12] A. B. Gaspar, G. Moln#r, A. Rotaru, H. J. Shepherd, *C. R. Chim.* 2018, *21*, 1095 – 1120.
[13] P. Guionneau, E. Collet in *Spin-crossover Materials: Properties and Applications*, Wiley, Oxford, 2013, pp. 507 – 526.
[14] T. Granier, B. Gallois, J. Gaultier, J. A. Real, J. Zarembowitch, *Inorg. Chem.* 1993, *32*, 5305 – 5312.
[15] P. Guionneau, C. Brigouleix, Y. Barrans, A. E. Goeta, J.-F. L8tard, J. A. K. Howard, J. Gaultier, D. Chasseau, *C. R. Acad. Sci. Paris Chim.* 2001, *4*, 161 – 171.
[16] H. J. Shepherd, S. Bonnet, P. Guionneau, S. Bedoui, G. Garbarino, W. Nicolazzi, A. Bousseksou, G. Moln#r, *Phys. Rev. B* 2011, *84*, 144107.
[17] H. J. Shepherd, T. Palamarciuc, P. Rosa, P. Guionneau, G. Moln#r, J.-F. L8tard, A. Bousseksou, *Angew. Chem. Int. Ed.* 2012, *51*, 3910 – 3914; *Angew. Chem.* 2012, *124*, 3976 – 3980.
[18] H. J. Shepherd, P. Rosa, L. Vendier, N. Casati, J.-F. L8tard, A. Bousseksou, P. Guionneau, G. Moln#r, *Phys. Chem. Chem. Phys.* 2012, *14*, 5265 – 5271.
[19] D. Pinkowicz, M. Rams, M. Misˇek, K. V. Kamenev, H. Tomkowiak, A. Katrusiak, B. Sieklucka, *J. Am. Chem. Soc.* 2015, *137*, 8795 – 8802.
[20] M. C. MuÇoz, J. A. Real in *Spin-Crossover Materials: Properties and Applications* (Ed.: M. A. Halcrow), Wiley, Oxford, 2013, pp. 121 – 146.
[21] M. C. MuÇoz, J. A. Real, *Coord. Chem. Rev.* 2011, *255*, 2068 – 2093.
[22] Z.-P. Ni, J.-L. Liu, Md. N. Hoque, W. Liu, J.-Y. Li, Y.-C. Chen, M.-L. Tong, *Coord. Chem. Rev.* 2017, *335*, 28– 43.
[23] V. Niel, A. L. Thompson, M. C. MuÇoz, A. Galet, A. E. Goeta, J. A. Real, *Angew. Chem. Int. Ed.* 2003, *42*, 3760 – 3763; *Angew. Chem.* 2003, *115*, 3890 – 3893.
[24] A. Galet, A. B. Gaspar, M. C. MuÇoz, G. V. Bukin, G. Levchenko, J. A. Real, *Adv. Mater.* 2005, *17*, 2949 – 2953.

[25] a) S. Decurtins, P. Ggtlich, P. C. Kçhler, H. Spiering, A. Hauser, *Chem. Phys. Lett.* 1984, *105*, 1 – 4; b) A. Hauser, *Chem. Phys. Lett.* 1986, *124*, 543 – 548.
[26] H. Schmidbaur, A. Schier, *Angew. Chem. Int. Ed.* 2015, *54*, 746 – 784; *Angew. Chem.* 2015, *127*, 756 – 797.
[27] L. Merrill, W. A. Bassett, *Rev. Sci. Instrum.* 1974, *45*, 290 – 294.
[28] A. Dawson, D. R. Allan, S. Parsons, M. Ruf, *J. Appl. Crystallogr.* 2004, *37*, 410 – 416.
[29] a) I. A. GuralQskiy, B. O. Golub, S. I. Shylin, V. Ksenofontov, H. J. Shepherd, P. R. Raithby, W. Tremel, I. O. Fritsky, *Eur. J. Inorg. Chem.* 2016, 3191 – 3195; b) B. R. Mullaney, L. Goux-Capes, D. J. Price, G. Chastanet, J. F. L8tard, C. J. Kepert, *Nat. Commun.* 2017, *8*, 1053.
[30] M. Ohba, K. Yoneda, G. Agust&, M. C. MuÇoz, A. B. Gaspar, J. A. Real, M. Yamasaki, H. Ando, Y. Nakao, S. Sakaki, S. Kitagawa, *Angew. Chem. Int. Ed.* 2009, *48*, 4767 – 4771; *Angew. Chem.* 2009, *121*, 4861 – 4865.